International Journal of Mass Spectrometry 304 (2011) 51–56

Contents lists available at ScienceDirect

International Journal of Mass Spectrometry

journal homepage: www.elsevier.com/locate/ijms

High-charge Coulomb explosions of clusters in ultra-dense deuterium D(−1)

Leif Holmlid*

Atmospheric Science, Department of Chemistry, University of Gothenburg, SE-412 96 Göteborg, Sweden

ARTICLE INFO

Article history:
Received 1 February 2011
Accepted 8 April 2011
Available online 15 April 2011

PACS:
61.46.Bc
73.22.−f
67.63.Gh
67.10.−j

Keywords:
Ultra-dense deuterium
Coulomb explosion
Time-of-flight
Cluster

ABSTRACT

Laser-induced Coulomb explosions of clusters D_N in ultra-dense deuterium D(−1) show a broad spectrum of fragmentation processes. For small clusters D_3 and D_4 symmetric fragmentation processes are often observed. Experiments now show that these clusters fragment by maximum-charge processes, like $D_4^{4+} \rightarrow 4D^+$, each fragment leaving with 945 eV kinetic energy. This is the case even at low laser pulse intensities of $<10^{12}$ W cm^{-2}. The facile laser field ionization of these clusters is probably caused by their small size. Such high-charge processes seem to be most common in the superfluid condensed phase. A centrifugal stretching in the clusters is observed, giving 5–8% longer D–D bonds at higher average laser intensity, probably at $J \leq 3$. Rotational excitation of D_2^+ fragments is often apparent at similar J values. This requires strong bonding between the two deuterons, predicted to be close to 700 eV due to strong exchange interaction.

1. Introduction

Ultra-dense deuterium D(−1) [1–8] is now studied with laser-induced neutral time-of-flight (TOF) energy measurements, using a new improved source for its production. The particles observed are released from the material by characteristic Coulomb explosions (CE). Due to the extremely high density of D(−1), of the order of 10^{29} cm^{-3} (140 kg cm^{-3}) it is clearly useful as target material for inertial confinement fusion (ICF) using intense pulsed lasers [5–8]. The ultra-dense material is only formed by deuterons, making the relatively clean fusion process D + D attainable more easily. The first experiments showing laser-induced fusion in D(−1) were recently described [8]. The main beneficial properties of D(−1) as fusion target are the extremely high density and especially the high-energy deuterons released in the material by CE processes.

Ultra-dense deuterium D(−1) consists of clusters of various forms, with strongly different modes of CE laser fragmentation. Large clusters are mainly in the form of chains of smaller clusters [9]. The typical fragmentation processes of such clusters are symmetric cleavage giving two identical fragments, each with half the kinetic energy release of 630 eV, and asymmetric processes giving one fast D fragment and a slow heavy fragment cluster. Here we investigate the CE processes for small clusters D_3 and D_4. This study is possible due to two innovations: (a) the novel source which removes TOF spectral overlap from other types of clusters and CE processes and (b) the deposition of D(−1) on a metal surface which cools and stabilizes the material under study.

The catalytic process in the emitter material forms dense deuterium D(1) which is converted into ultra-dense deuterium D(−1) [1,2]. D(1) is similar to H(1) [10]. The excitation level for Rydberg matter [11–14] of D is generally indicated as D(l), where l is the angular momentum quantum number. The basis for the description of D(−1) is that this material is an inverted form of D(1), where deuterons and electrons have exchanged their roles. This is based on the general ideas of dense hydrogen materials by Ashcroft and other authors [15,16]. The reason for this inversion is probably the fact that the deuterons are bosons and thus do not resist the inversion to the ultra-dense material. The quantum mechanical basis for D(−1) was recently discussed by Winterberg [17,18], suggesting the formation of vortices in a Cooper pair electron fluid to give the large electron mass required for the inverted material.

2. Theory

The method used here to measure the bond distances in D(−1) is laser-induced Coulomb explosions (CE) [1,2,5]. The 5 ns long laser pulse excites electrons in the material to give bare nuclei exposed to their full Coulomb repulsion. This may mean an ionization process but may also only involve an excitation (displacement) of the shielding electrons from the conduction band into higher localized

* Tel.: +46 31 786 9076.
E-mail address: holmlid@chem.gu.se

1387-3806/$ – see front matter © 2011 Elsevier B.V. All rights reserved.
doi:10.1016/j.ijms.2011.04.001

Table 1
Fragmentation of small D(−1) clusters with three or four closely located ion charges. Fragment mass is 2u if not otherwise indicated.

Type/Name	Total cluster mass	E_1 (eV)	E_2 (eV)	E_3 (eV)	E_4 (eV)	t_1 (ns)	t_2 (ns)	t_3 (ns)	t_4 (ns)
Symmetric									
12(3+)S	12	630 (4u)	630 (4u)	630 (4u)		582	582	582	
8(4+)S	8	945	945	945	945	336	336	336	336
6(3+)S	6	630	630	630		412	412	412	
Asymmetric 120°									
10(3+)A	10	473 (4u)	473 (4u)	945		671	671	336	
8(3+)A	8	378 (4u)	756	756		751	375	375	
Linear									
6(3+)L	6	788	0	788		368	–	368	

(non-shielding) orbitals in the condensed material. The potential energy between two exposed charges is

$$W = \frac{e^2}{4\pi\varepsilon_0 d}. \quad (1)$$

where d is the distance between the two ionic fragments. This energy is transformed to kinetic energy between the two ionic fragments during their mutual repulsion. This kinetic energy release (KER) may appear as kinetic energy in one light fragment, ejected from a large cluster. For D(−1), the KER is often observed as kinetic energy in two different fragments, and the relative masses of the fragments will determine their fraction of the KER. Calculations of such energy fractionation are used for the interpretation of the results here.

The CE fragmentation processes in the material D(−1) indicate a common KER of 630 eV [1,2,5]. This means an interatomic distance of 2.3 ± 0.1 pm, a factor of approximately 65 smaller than in the D(1). Several fragmentation processes are summarized in Tables 1 and 2, where the data in Table 2 are mainly for reference purposes. These results are verified experimentally in other studies, but several entries are just for reference and have not been observed experimentally. Here, we will describe the results in Table 1 which are most relevant for the results given below.

A small cluster with three positive charges created by field ionization will fall apart to three recoiling ions in a quite complex way, depending on the initial geometry of the cluster. In the case of a D_3 cluster, the problem of the energy release (energy given to each D^+ fragment) is easily solved if the ionized cluster is perfectly symmetric in the D_{3h} point group. The energy of each fragment is then one third of the total repulsion energy, being 3 × 630 eV = 1890 eV. Any initial asymmetry like in a C_{2v} form gives other fragment energies. Assuming that one of the fragments is leaving along the C_2 symmetry axis and the other two leave at the same angle θ towards the symmetry axis, one can find an expression for the kinetic energy of the odd fragment (moving along the symmetry axis, index 3) as

$$E_3 = \frac{2E}{(3 + \tan^2\theta)} \quad (2)$$

where E is the total repulsion energy, here 1890 eV. This formula is thus valid for three equal masses. With $\theta = 60°$ thus a D_{3h} case, $E_3 = E/3$ is found correctly. This symmetric case is shown in Table 1 as 6(3+)S, with 6 indicating the total mass of the cluster. It is likely that a slight asymmetry of the initial cluster will give a spread of kinetic energies to the fragments, possibly contributing to the peak width for the symmetric process 6(3+)S. The entry for symmetric fragmentation of a possible D_6 cluster in Table 1, called 12(3+)S is found in the same way from Eq. (2).

Assuming other masses, it is possible to derive similar formulas for 4- and 5-atom clusters. Assuming that the odd mass is always receding along the C_{2v} symmetry axis, thus $m_3 = 4u$ for a 4-atom cluster and $m_3 = 2u$ for a 5-atom cluster, the derivations are simplified. For a 4-atom cluster D_4 one finds

$$E_3 = \frac{E}{(2 + \tan^2\theta)} \quad (3)$$

and for a 5-atom cluster

$$E_3 = \frac{4E}{(5 + \tan^2\theta)} \quad (4)$$

The entries 8(3+)A and 10(3+)A are found from these formulas, assuming $\theta = 60°$. In these cases, it is not clear that this angle of recoil will be the preferred one, and different values of kinetic energy for the fragments than the ones given in Table 1 exist.

Another mode of recoil is possible in the case of a D_3 cluster, if the cluster is initially in the linear $D_{\infty h}$ form. In that case, the total energy is smaller, 1575 eV, and it is possible that the central ion is stationary and that each receding ion receives 788 eV from the repulsion. This is the final entry in Table 1.

Table 2
Asymmetric and symmetric fragmentation of D(−1) clusters. Many of these fragmentation processes have been observed in previous experiments (to be published).

Total charge	Total cluster mass	Name	t_1 (ns)	t_2 (ns)
Asymmetric				
2	∞	2←→∞	412	
	16	2←→14	440	3080
	14	2←→12	445	2667
	12	2←→10	451	2254
	10	2←→8	460	1841
	8	2←→6	475	1486
	6	2←→4	504	1008
	12	4←→8	713	1426
	10	4←→6	752	1127
3	∞	2←→∞ (2+)	291	
	16	2←→14 (2+)	311	2178
	14	2←→12 (2+)	314	1886
	12	2←→10 (2+)	319	1594
	10	2←→8 (2+)	325	1302
	8	2←→6 (2+)	336	1008
	6	2←→4 (2+)	357	713
Symmetric				
2	12	6←→6	1008	1008
	8	4←→4	823	823
	4	2←→2	582	582

3. Experimental

The new source part is shown in the schematic drawing in Fig. 1. It is recently described in detail in Ref. [19]. The RM emitter is as in previous studies a cylindrical (extruded) sample of an industrial iron oxide catalyst doped with K (initially at 8 wt%) [20,21]. It is of the (obsolete) styrene catalyst type Shell S-105 which is a hydrogen abstraction and transfer catalyst. The catalyst is mounted and held in place with a small screw in the tight-fitting opening of a metal tube which is connected to the D_2 gas feed. In this way, the deuterium has to diffuse through the porous catalyst or directly above the catalyst surface before diffusing out into the vacuum chamber and being pumped away. This gives efficient formation of D(−1) in the emitter. The metal (Pt) tube with 6 mm outer diameter and

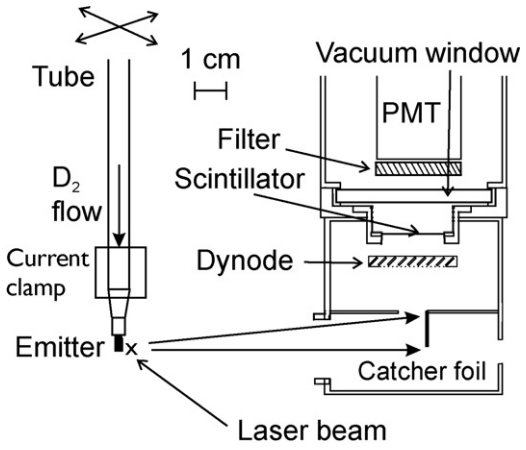

Fig. 1. Cut through source and detector at 90° towards the laser beam. In some experiments, the emitter was lifted above the laser beam and centered. The laser beam then interacted with the D(−1) layer on a stainless steel surface below the emitter.

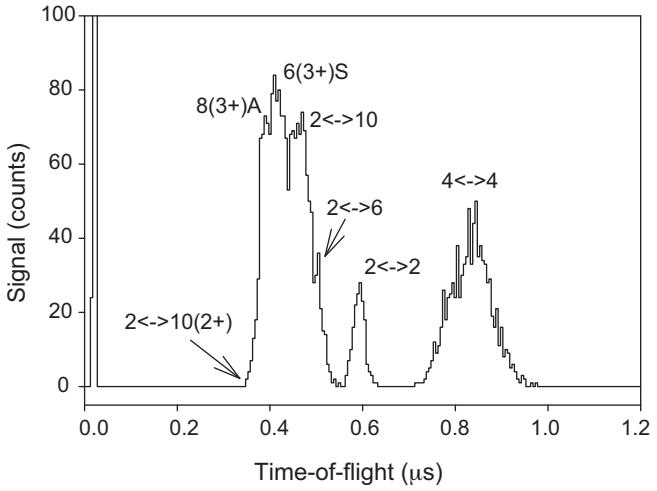

Fig. 2. Typical TOF spectrum from the source, with laser beam close to the emitter as shown in Fig. 1. The broad peak 4←→4 probably contains further unresolved features.

wall thickness of 100 μm is heated by an AC current though its wall, with the upper end at the vacuum wall at zero potential. The lower end is connected to a Cu clamp and thick flexible Cu braids which supply the AC current. This clamp also tightens the Pt tube against the emitter holder tube. The current through the tube is up to 28 A, at a total power of 22 W. The D_2 gas is heated by the tube. The highest emitter temperature reached is 475 K (200 °C) at 28 A. The base pressure in the vacuum chamber is 1×10^{-6} mbar. Deuterium gas (>99.8% D_2) is admitted at a pressure in the chamber up to 1×10^{-5} mbar. In some of the experiments described, a stainless steel surface is mounted below the emitter so that D(−1) forms a layer on its surface.

A Nd:YAG laser with an energy of <200 mJ per each 5 ns long pulse at 10 Hz is used at 532 nm. The laser beam is focused with an $f = 400$ mm spherical lens at the center of the UHV chamber. The intensity in the beam waist of (nominally) 70 μm diameter is relatively low, $\leq 10^{12}$ W cm^{-2} as calculated for a Gaussian beam. The detector is a dynode-scintillator-photomultiplier setup that is described in detail elsewhere [10] and shown in Fig. 1. The detector is here located at an angle of 45–60° from the incoming laser beam and measures the time-of-flight (TOF) spectra of neutral particles since no accelerating voltage is employed. The fast particles impact on a stainless steel foil in the detector, and fast ions ejected from there are drawn towards a Cu–Be dynode held at −7.0 kV inside the detector. The photomultiplier (PMT) is Electron Tubes 9128B with single electron rise time of 2.5 ns and transit time of 30 ns. Blue glass filters in front of the PMT strongly decrease the pulsed laser light signal observed by the PMT. The signal from the PMT is collected by a multi-channel scaler (EG&G Ortec Turbo-MCS) with preamplifier. The dwell time per channel used here is 5 ns. Each spectrum consists of a sum of the fragment signals from 250 laser shots. In some experiments, the laser samples the layer of D(−1) on the steel surface below the emitter.

Since the particles observed are only accelerated by the CE and not by any voltage in the apparatus, the TOF calibration cannot use known ions. Due to the high kinetic energy of the particles detected here, they are not deflected by the dynode potential in the detector like slow ions but instead hit the catcher foil inside the detector, from which positively charged particles are ejected or scattered. The distance to this foil from the laser waist or point of interaction is the particle flight distance, nominally 101 mm. Internal calibration for example with the 2←→2 peaks (see below) has been done with reliable results. The error in the TOF may be of the order of 10 ns from this, which is the error likely from the MCS channel start. The match of different peaks to calculated TOF is good, and there is no indication of any error larger than 10 ns in the calibration.

4. Results

A typical TOF spectrum is shown in Fig. 2, with interpretation based on the calculated results both in Table 1 for the CE processes described in Section 2 and in Table 2 for CE processes identified previously [1–8]. Several entries in Table 2 are included for comparison and checking purposes and are not normally observed. In Fig. 2, the limit to short TOF indicated may also have other reasons, but a reasonable interpretation is provided in the figure in agreement with previous studies. However, the important information is in the peaks and their interpretation. The peaks indicated as 8(3+)A, assigned to fragmentation of clusters D_4, and 6(3+)S assigned to D_3 fragmentation are of special interest. The D_3 fragmentation is likely to give a symmetric recoil pattern for the three D^+ ions, and the energy is given in Table 1. A small disturbance in the symmetry of the D_3^{3+} complex will give asymmetric recoils and thus slightly different energies. The width of the peak may be due to such effects. The D_4 fragmentation here gives two D^+ ions and one D_2^+ ion, and the energy given to each fragment varies with the angles of recoil. In Table 1, the case with all fragments leaving at 120° to each other is assumed, but a spread of recoil angles will exist. Thus, the assignment of the *asymmetric* process 8(3+)A is only tentative.

To help in the interpretation of the TOF spectra in the figures, Fig. 3 shows the TOF data from Tables 1 and 2 in a condensed form. The spectra according to this view contain two broad peaks and two sharper peaks 2←→2 and 4←→4. However, due to more complex processes forming the 4←→4 peak, also this peak is usually rather broad. As will be shown below, the intensity due to the asymmetric processes giving one fast D^+ fragment is relatively low in the

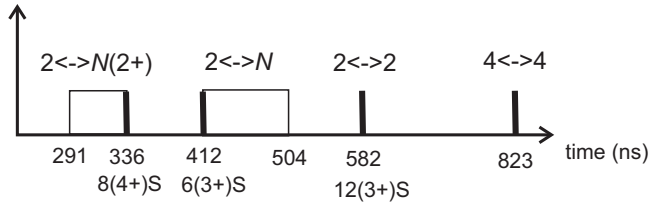

Fig. 3. A summary of the main TOF peaks observed, not to scale. See further Tables 1 and 2.

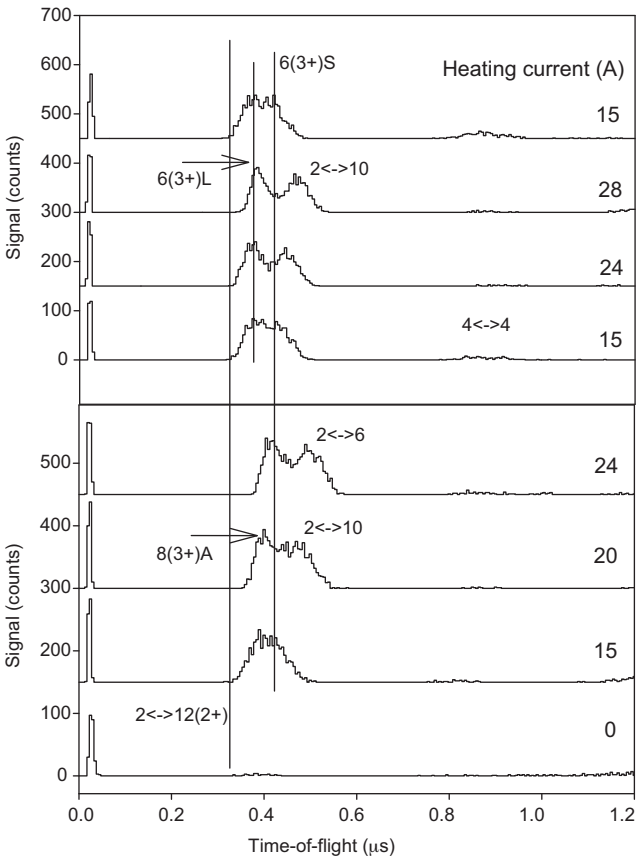

Fig. 4. Variation of cluster formation with heating of the source. The heating current is used as parameter. The two panels show two different experiments, each one starting at the bottom spectrum and progressing upwards.

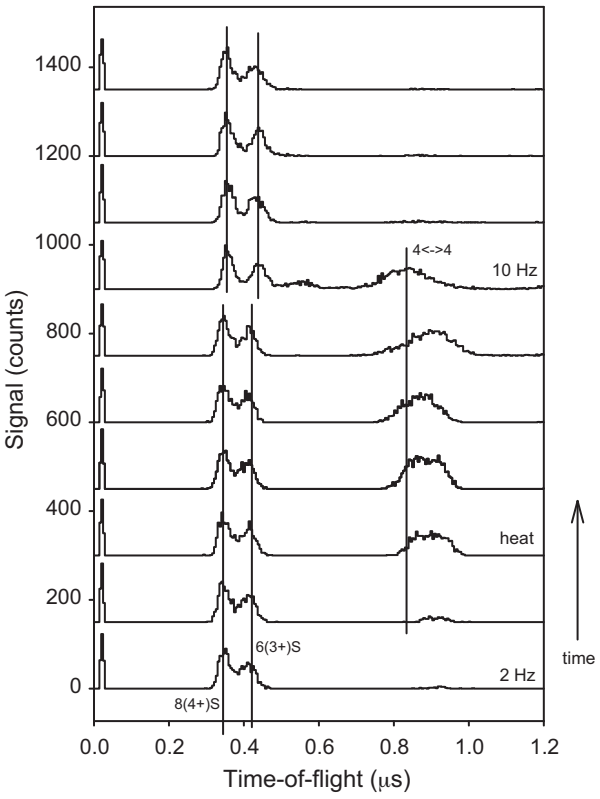

Fig. 5. An experiment with increasing source temperature and laser pulse frequency. The laser samples the layer of D(−1) on a metal surface below the emitter. The small shifts of the two fastest TOF peaks may indicate a larger bond distance due to the energy deposition from the laser and the source heating. Time scale recalculated from 98 to 101 mm flight distance.

present type of experiment, and the fast peaks are mainly due to the symmetric 8(4+)S and 6(3+)S processes.

The fragmentation patterns vary with the conditions for formation of the clusters. In Fig. 4, the influence of the source temperature is shown. At high temperature, clusters giving asymmetric fragmentation like the process 2←→10 seem to be formed. This is a CE process $D_6^{2+} \rightarrow D_5^{+} + D^{+}$. The results indicate that large clusters are built up at high temperature, while small clusters D_3 and D_4 are mainly detected at low temperature.

For the present study of small cluster fragmentation, it is necessary to have good TOF calibration and to form the small clusters at large densities. These two points have been solved by studying the CE processes on a solid surface covered with D(−1), where the point of laser interaction is better defined than in the cluster phase outside the emitter. The experiments in Figs. 5 and 6 are of this type. The TOF distance was in this case 98 mm due to the size of the solid surface, slightly shorter than the 101 mm used from the center of the apparatus. The time scale in these figures is recalculated to 101 mm flight distance to simplify the comparison with theory and other experiments. In Fig. 5, an experiment where the conditions are changed from the normal 2 Hz laser repetition to 10 Hz, with increased heating of the D(−1) material is shown. Different small retardations of the two fast TOF peaks are observed at the higher laser pulse rate, besides changes in the structure of fragmentation 4←→4 thus of the CE process $D_4^{2+} \rightarrow D_2^{+} + D_2^{+}$. Results from this figure are included in Table 3, giving the energies of the TOF peaks and the corresponding D–D bond distances. In Fig. 6, the reverse situation is studied with a decreased influx of heat from the source with time. The fast peaks shift to shorter times in this case. The slower peaks, which partly are due to 4←→4 and 2←→2, change in several steps during the apparent stabilization of the material, in the end giving only one TOF peak corresponding to delayed fragments from the 4←→4 process.

5. Discussion

The two processes 10(3+)A and 8(3+)A in Table 1 are not observed with certainty. This means that the results presented here do not give any proof for asymmetric CR processes of the small D(−1) clusters. Of course, the energy and time values given in Table 1 are only tentative, since the angle of fragmentation assumed at 60° towards the C_{2v} symmetry axes may not be applicable. It is likely that a spread of such angles exist, which may give low and broad TOF peaks for these CE processes. The linear CE form 6(3+)L may exist, as shown in Fig. 4, but this assignment is not final. The main processes observed are the symmetric processes 8(4+)S and 6(3+)S in Table 1.

There exists a tendency for these symmetric CE processes in small clusters to be more common in the liquid (surface) phase studied in Figs. 5 and 6, while the gas (cluster) phase observed in

Table 3
Calculated results from the TOF peaks in Fig. 5. The bond length for the first peak is found after reducing the nominal fragment energy by the factor 2/3 to normalize to the D^+–D^+ repulsion energy.

Laser frequency (Hz)	1st peak 8(4+)S from D_4	2nd peak 6(3+)S from D_3
10 Hz	970 eV 2.23 pm	620 eV 2.32 pm
2 Hz	1020 eV 2.12 pm	670 eV 2.15 pm

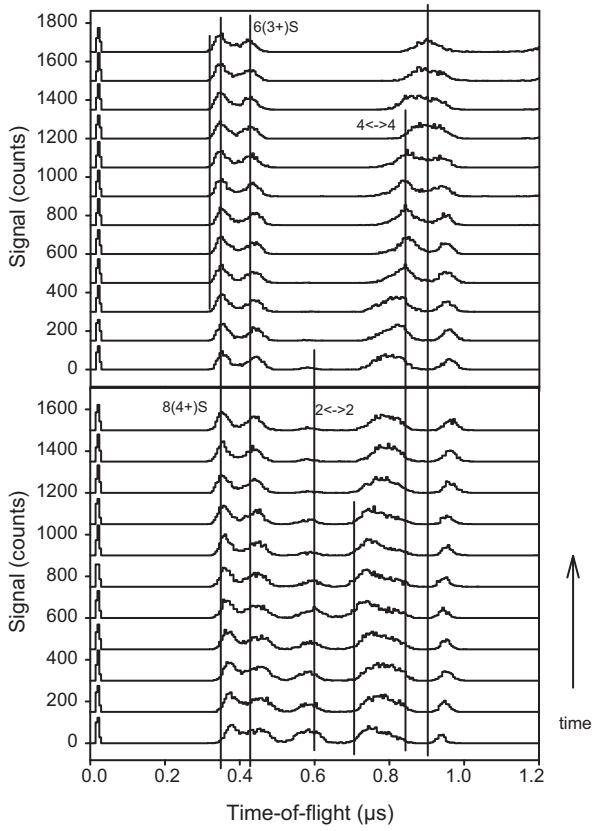

Fig. 6. Experiment with decreasing source heating, sampling the D(−1) layer adsorbed on a surface below the emitter. D_2 admission. 25 A heating current in the lower panel, no heating in the upper panel. Several TOF peaks change structure or disappear due to the cooler material, indicating a structure mainly formed by D_3 and D_4 at the end of the experiment. Time scale recalculated from 98 to 101 mm flight distance.

Figs. 2 and 4 also give other processes for larger clusters. This is not believed to be the full picture, but the small clusters observed by CE in the liquid phase may be end groups or weakly bound clusters forming the chains of clusters which are observed in the gas phase. Different processes are anyway observed in the cluster and liquid phases. For example, the process 8(4+)S does not exist under the conditions of Fig. 4. Thus, the distributions of the cluster sizes and shapes, or at least the fragmentation patterns change with the physical environment, apparently showing larger (longer) clusters in the cluster phase, and smaller clusters, mainly D_3 and D_4 in the liquid adsorbed layer of D(−1) on a metal surface. The adsorbed D(−1) layer is probably superfluid [6,17,18]. Indeed, large clusters do exist also in the liquid phase since they can be observed at longer TOF, but their form is not so easily observed by TOF in such cases. Considering that the superfluid phase should contain quantum vortices which may have some structural cause, one might suggest that the formation of long chain clusters by interaction between small symmetric clusters could be coupled to such vortices.

Many changes in the TOF spectra due to external parameters like laser intensity and temperature can be understood as real changes in the clusters structure and the CE processes taking place, like the changes in the peak structure in Fig. 4 and for the slower peaks in Figs. 5 and 6. However, the shifts in Figs. 5 and 6 for the two fast peaks do not have such an explanation. Instead, one process that could be expected to give such a behavior in Fig. 5 is an increase in the temperature of the D(−1) surface layer due to the higher laser average intensity. The data in Fig. 5 indicate a change in the D–D distance in the D_3 cluster from 2.15 pm at the low laser pulse frequency to 2.32 pm at the high laser pulse frequency. This second value is in good agreement with the initial results on D(−1) published [1,2], probably since the laser conditions were similar. The large observed change of 5-8% in the bond distance with this change in the laser parameter is not expected for any ordinary bond in a cluster or molecule. It may indicate a highly asymmetric potential for the bonding, with a very steep barrier at short distance (the nuclear barrier) and a much slower variation at longer distances. The observed size of this effect may also be considered to be very large, however, the temperature increase in the material is not known. The peak width in Fig. 5 corresponds to a temperature of 60 000 K (6 eV) at least, but this broadening may mainly be due to a slight asymmetry in the CE process and not to a high temperature.

There is, however, another effect which may explain the observations and which is based on the quantum mechanical description of the superfluid material. This effect is quantized rotation due to the vortices in the superfluid. If a long cluster chain is spinning around its axis (the quantum vortex), the centrifugal force will easily stretch the bonds. This is a well-known effect in spectroscopy called centrifugal stretching and the main cause which gives shifts in bond lengths for molecules [22]. With a slow variation of the potential towards longer bond distance as assumed above, the retaining force is rather small so the 5–8% change in distance observed here appears entirely possible. We conclude that the observed stretching is likely due to centrifugal effects. Due to the extremely small moment of inertia for a $D_2(-1)$ pair, even a relatively low rotational angular momentum gives high rotational energy which may stretch the bonds considerably. For example, $J = 1$ gives 7.8 eV rotational energy. This requires a strong bonding between the deuterons in the clusters, so that they do not fall apart in the rotation. The exchange force between deuterons was recently derived by Winterberg [17]. The value found at a distance of 2.3 pm from the formula given there is −720 eV, thus attractive and large enough give stable pairs of D_2 which can rotate with high energy. The shorter bond distances in Table 3 for the D_4 cluster relative to the D_3 cluster is in agreement with what is expected for exchange forces, where a larger number of deuterons will interact more strongly.

In many of the TOF spectra, special features appear for the 4←→4 peaks. In the case in Fig. 5, the peak is delayed until the laser pulse frequency is changed to 10 Hz. The delayed peaks have approximately 50 eV lower kinetic energy, presumably due to transfer of some of the KER to rotational energy in the CE process. It is possible that the D_2^+ fragments indeed become rotationally excited by a slightly asymmetric fragmentation process. Due to the very small moment of inertia for a $D_2(-1)$ pair, low angular momentum gives a large rotational energy and $J = 3$ gives 47 eV rotational energy. An exchange force between the deuterons as discussed above makes this possible. If the bond D–D would break due to too fast rotation (not by ionization or CE in the D_2 pair), the fragments would arrive at an average TOF of 823 ns. This may be what is observed in Fig. 5 when the laser pulse frequency is increased to 10 Hz, and the full D_2^+–D_2^+ repulsion energy is observed with a TOF of 823 ns. The reverse is observed in Fig. 6 where the final slow peak is found to correspond to a delayed 4←→4 process.

6. Conclusions

It is shown that small clusters D_3 and D_4 exist in a surface layer of ultra-dense deuterium D(−1), probably partially in long cluster chains which correspond to the quantum vortices in the superfluid material. These clusters are easily ionized by a pulsed laser at relatively low intensity. The clusters fragment by Coulomb explosions between three or four ion charges, corresponding to the maximum charge of the clusters. The energy of the D^+ fragments is high, up to 945 eV. A centrifugal stretching effect in the clus-

ters is observed, giving longer D–D bonds at higher average laser intensity and higher source temperature. D_4 clusters also form D_2^+ fragments, which can be highly rotationally excited. The existence of fast and rotating D_2^+ fragments indicates a strong attractive exchange interaction between two deuterons, as predicted theoretically.

References

[1] S. Badiei, P.U. Andersson, L. Holmlid, Int. J. Hydrogen Energy 34 (2009) 487.
[2] S. Badiei, P.U. Andersson, L. Holmlid, Int. J. Mass Spectrom. 282 (2009) 70.
[3] P.U. Andersson, L. Holmlid, Phys. Lett. A 373 (2009) 3067.
[4] L. Holmlid, H. Hora, G. Miley, X. Yang, Laser Part. Beams 27 (2009) 529.
[5] S. Badiei, P.U. Andersson, L. Holmlid, Phys. Scr. 81 (2010) 045601.
[6] P.U. Andersson, L. Holmlid, Phys. Lett. A 374 (2010) 2856.
[7] S. Badiei, P.U. Andersson, L. Holmlid, Appl. Phys. Lett. 96 (2010) 124103.
[8] S. Badiei, P.U. Andersson, L. Holmlid, Laser Part. Beams 28 (2010) 313.
[9] P.U. Andersson, L. Holmlid, Phys. Lett. A. 375 (2011) 1344.
[10] S. Badiei, L. Holmlid, J. Phys. B: At. Mol. Opt. Phys. 39 (2006) 4191.
[11] É.A. Manykin, M.I. Ozhovan, P.P. Poluéktov, Sov. Phys. Tech. Lett. 6 (1980) 95.
[12] E.A. Manykin, M.I. Ojovan, P.P. Poluektov, Proc. SPIE 6181 (2006) 618105-1-9.
[13] É.A. Manykin, M.I. Ozhovan, P.P. Poluéktov, Sov. Phys. JETP 75 (1992) 440.
[14] L. Holmlid, Chem. Phys. 237 (1998) 11.
[15] N.W. Ashcroft, J. Low Temp. Phys. 139 (2005) 711.
[16] B. Militzer, R.L. Graham, J. Phys. Chem. Solids 67 (2006) 2136.
[17] F. Winterberg, J. Fusion Energy 29 (2010) 317.
[18] F. Winterberg, Phys. Lett. A 374 (2010) 2766.
[19] P.U. Andersson, B. Lönn, L. Holmlid, Rev. Sci. Instrum. 82 (2011) 013503.
[20] G.R. Meima, P.G. Menon, Appl. Catal. A 212 (2001) 239.
[21] M. Muhler, R. Schlögl, G. Ertl, J. Catal. 138 (1992) 413.
[22] J.M. Hollas, High Resolution Spectroscopy, 2nd ed, Wiley, Chichester, 1998.